

The Application of CFD to the Multi-Scale Characterization of Anti-Solvent Addition Crystallizations

Mark Barrett, Des O' Grady, Brian Glennon & Eoin Casey

School of Chemical and Bioprocess Engineering,

Centre for Synthesis and Chemical Biology,

University College Dublin, Belfield, Dublin 4, Ireland

Introduction

Anti-solvent crystallization can be used as an alternative to cooling or evaporation for the separation and purification of solid product in the pharmaceutical industry. Addition of anti-solvent reduces the solubility of a solute in solution thereby facilitating the generation of supersaturation, the driving force for nucleation and growth. Some of the problems associated with anti-solvent crystallization are that it is poorly understood, can produce fine irregularly shaped crystals and is prone to the formation of polymorphs, solvates and hydrates.

The scale up of anti-solvent crystallization is particularly difficult due to the importance of mixing in the system. An increase in the intensity of mixing can maintain a better crystal suspension, reduce the degree of settling and improve the impurity profile. However, the same increase may entrain air from the headspace, increase the level of attrition and cause shear damage to the crystals. Mixing intensity can also affect the growth and nucleation kinetics of the system. For anti-solvent crystallization an additional challenge associated with mixing is the need to blend anti-solvent and solution phases rapidly, so as to ensure a homogenous level of supersaturation throughout the vessel. Additionally, the change in systems blend time and velocity profiles can be problematic on scale up. The application of Computational Fluid Dynamics (CFD) to help understand and characterize the mixing¹⁻⁴ within all scale of vessels is therefore a necessity to understand and allow for "right first time" scale up.

To characterize anti-solvent crystallization the use of in-line tools is vital. Focused Beam Reflectance Measurement (FBRM) can be used to monitor key properties relating to the size and number of crystals in a crystallizer. FBRM has been used to measure solubility and metastable zone width (MSZW) data^{5,6}, monitor nucleation kinetics⁶, measure particle size⁷ and assess the effect of temperature cycling⁸ and impurities⁹. Attenuated Total Reflectance Fourier Transform Infrared spectroscopy (ATR-FTIR) can be used to measure the concentration of both solute and anti-solvent in solution. It has been used to monitor supersaturation¹⁰ assess the impact of seeding¹¹ and identify oiling out phenomena¹². These in-line tools eliminate the need to sample. A sample may not be representative and there is also the possibility that crystallization may continue between sampling and analysis. Additionally, many off-line methods need the sample to be altered in some way (i.e. dilution, sonication) and this may impact on effective analysis. These methods provide in-line real time data that can be

combined with CFD to provide an extremely useful picture of what is happening inside a crystallizer at any point in the batch.

With the information gained it is possible to assess the impact of many process variables and chose suitable operating parameters to provide the most robust scale up strategy (i.e. 'The Scale up Tool Box'). This paper outlines this semi quantitative approach to crystallization understanding, at the bench scale, and its application to scale up.

Experimental Methods

The crystallization of benzoic acid, from an ethanol-water solution, with water as the anti-solvent, was examined. Benzoic acid is highly soluble in ethanol (58.36 g/100g @ 25°C) and importantly is insoluble in water (0.25g/100g @ 25°C) ¹³. The crystallization characteristics assessed, including CLDs (Chord Length Distributions), MSZWs (Meta Stable Zone Widths) and image analysis were all carried out at 25°C.

A solution of 75g water, 75g ethanol and 21g benzoic acid, was held at 25°C in a 500 mL glass jacketed vessel with a Julabo chiller fitted for temperature control. A motor driven, pitched blade impeller provided agitation. FBRM (model S400), ATR-FTIR (reactIR 4000) and temperature probes were placed in the vessel to monitor the crystallization and as a consequence provided baffling (see Figure 1). This baffling was sufficient to avoid excessive vortexing and hence air entrainment into the bulk solution was not an issue at this scale. Water at 25°C was fed to the vessel at a variety of rates (0.05 gs⁻¹, 0.14 gs⁻¹, 0.24 gs⁻¹, 0.34 gs⁻¹ and 0.48 gs⁻¹). Two addition location of anti-solvent were examined. Feed point 1 ('near addition'), which is located close to the impeller shaft and feed point 2 ('far addition'), which is located beside the reactor wall.

Nozzle addition was also investigated in an effort to overcome poor mixing in the region close to the reactor wall. This involved reducing the feed pipe diameter from 5 mm to less the 1mm. The effect of both an increase in anti-solvent exit velocity and reduction in the droplet diameter, on the MSZ and CLDs was examined.

All experiments were performed in triplicate and the reported values are the mean of the three experiments. FBRM was used to pin point the time of nucleation and allowed for the MSZ to be characterized at the different addition rates, location and mode.

The following figure 1 outlines the orientation of the *in-situ* tools and the anti-solvent feed point locations assessed.

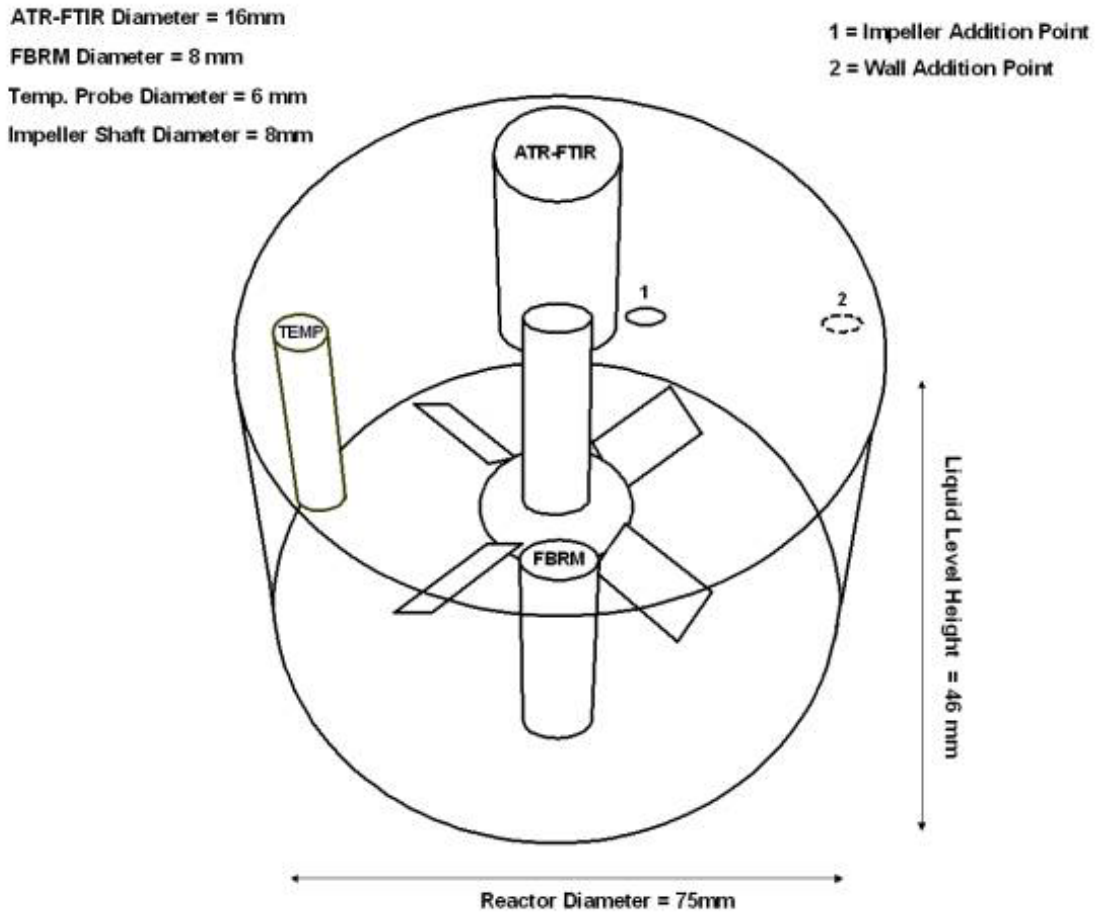


Figure 1: Feed position 1 - close to the impeller; Feed position 2 – close to the wall

Computational Fluid Dynamic Models

To investigate the velocity profiles prior to nucleation, the system is treated as a single phase and the possible solid-liquid interactions after nucleation are not considered. Initially, the 500 ml vessel, and its complex baffling system (the FBRM, REACT-IR and temperature probes), were constructed within GAMBIT 2.1.6. The precise geometry and dimensions of the system (pitch blade impeller, probes *etc.*) were created in the graphical user interface (GUI) allowing for the meshing of the vessel and its internals, along with the assigning of zone types and system specifics (*i.e.* fluid viscosity, internal reactor temperature and agitation speed).

The system contained 823 individual volumes and $\sim 475,000$ cells. A structured hexahedral meshing scheme was applied, as less numerical diffusion errors are evident than in a tetrahedral-based mesh. The mesh created in GAMBIT was then exported to FLUENT 6.1.2 for solution of the momentum and continuity equations for the turbulent flow within the crystallizer. The 'Multiple Reference Frame' (MRF) approach is applied to the system and the flow equations solved using the SIMPLE algorithm. The Reynolds number for the agitation speeds assessed lie between $\sim 12,500$ (325 rpm) and $\sim 18,500$ (475rpm). The standard k-epsilon turbulence model was chosen to model the flows. In addition, a no-slip boundary

condition was imposed on all walls and the free liquid surface was modelled with no vortex, a zero-flux and zero-stress conditions. To initially validate the model the tip speed of the impeller was calculated and compared to the tip speed calculated using the model. The model underestimated the tip speed by about 3% at 325 and 250 rpm indicating the model was suitable.

Currently the CFD simulations produced at the 70 L scale are being validated through 'Hot Film Anemometry'. Early results correspond well to the predicted CFD velocities within the pilot scale crystallizer.

Experimental Results

Case Study 1: Increased Process Understanding through CFD and *In-situ* Tools

The effect of addition rate and addition location on the MSZW has previously been examined within the same research group. This work suggests that for an addition point close to the impeller the MSZW widens as addition rate increases. Increasing the agitation intensity narrows the MSZW at all addition rates. These experiments proved repeatable indicating that this addition regime resulted in a robust experiment at both the high and low agitation levels.

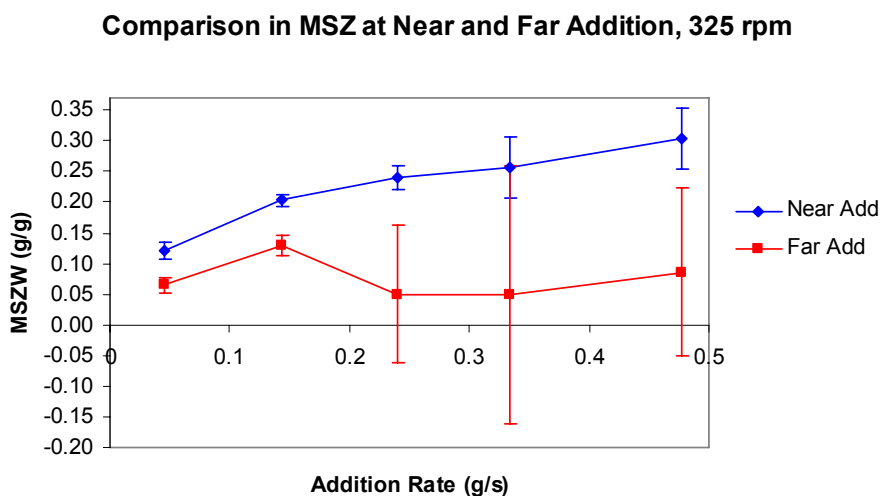


Figure 2: Effect of feed point location on MSZW at 325 rpm

Comparison in MSZ at Near and Far Addition, 250 rpm

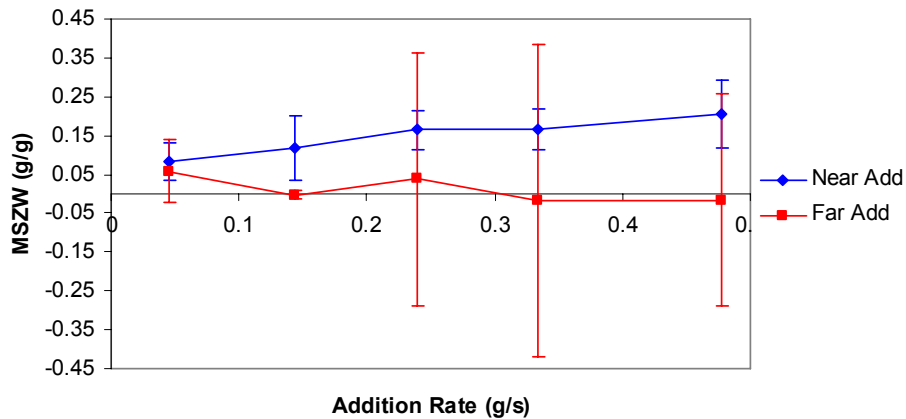


Figure 3: Effect of feed point location on MSZW at 250 rpm

Figures 2 and 3 also show the effect of addition location on the MSZW. Premature nucleation is evident at this 'far' feed location. In this region, due to poor anti-solvent dispersion, supersaturation levels reached close to the feed pipe allow for the onset of nucleation prior to a change in the bulk solutions solubility. In addition, at the 'far' addition location there are substantial fluctuations in the MSZW data produced highlighting the lack of repeatability of these experiments. This data emphasizes the importance of feed point location and the impact it can have on the systems crystallization characteristics.

With this in mind Computational Fluid Dynamics (CFD) was applied; with the aim of quantitatively describing the fluctuations on the data produced between the 'near' and 'far' feed point locations. It is at the point of nucleation that the addition location is of the most importance, as it is at this stage that it is desirable to minimise local areas of high supersaturation and thus minimise the probability of inducing premature nucleation. With the MSZW knowledge gained it was possible to predict the region that the systems would nucleate, therefore the nucleation volume could be simulated. These simulations are based on liquid-liquid systems and do not incorporate events following nucleation (i.e. solid suspension and solid-liquid interact)

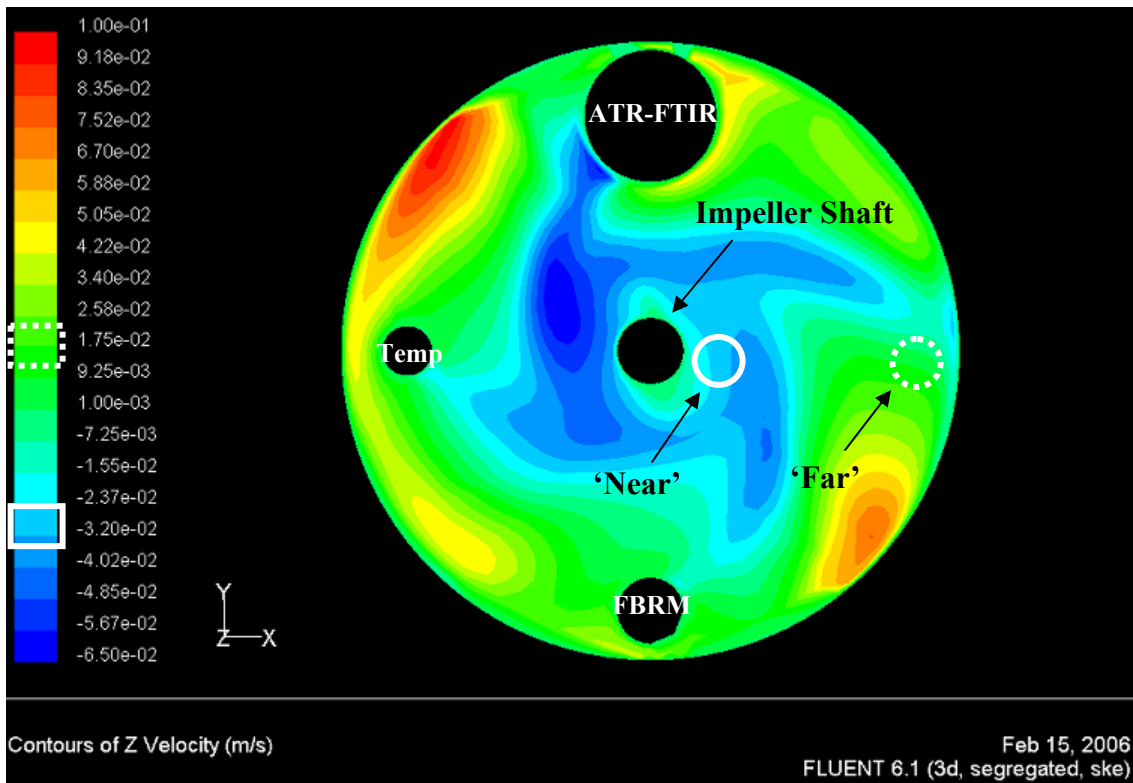


Figure 4: Z-velocity (i.e Upward and downward velocities) profile at nucleation volume at 325 rpm.

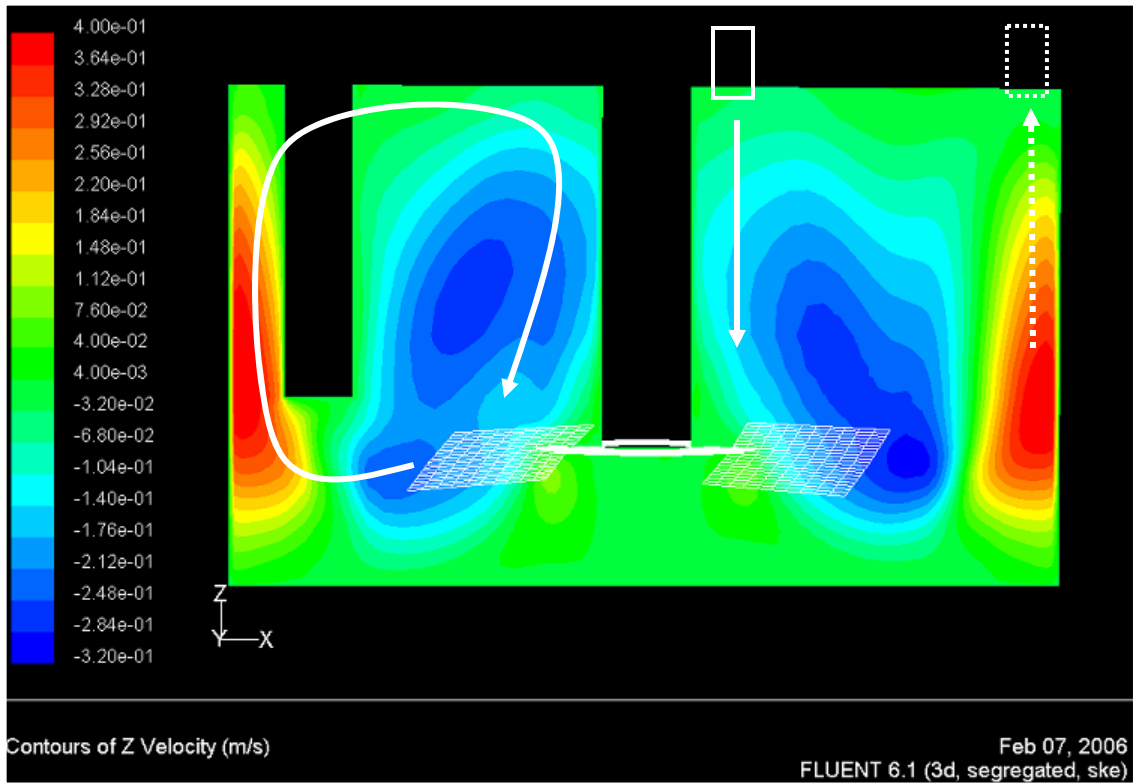


Figure 5: Z-velocity (i.e. Upward and downward velocities) profile at nucleation volume at 325 rpm. Vertical section through crystallizer showing mixing pattern and velocity directions at feed points.

It is important to assess the velocity in the z-direction (i.e. velocities in the upward or downward direction) for above surface addition, as it is important in determining the time taken to incorporate and homogeneously disperse the anti-solvent into the bulk solution (blend time). It is evident from figures 4 and 5 that the velocities at the 'near' feed location are in the downward or negative direction, in comparison to the velocities at the 'far' location, which is in a region of upward dominating velocities. Locating the feed point close to the reactor wall has in turn prevented the immediate incorporation of the anti-solvent into the bulk solution. As the velocities in this area are positive it will allow for liquid 'hold-up' and thus an increase in the regions local supersaturation. As the MSZW data indicates the supersaturation generated, at the 'far' feed point, is sufficiently high to induce premature nucleation of the benzoic acid system. To quantitatively examine this liquid 'hold-up', or the delay in the dispersion of the anti-solvent at the 'far' feed point location, mixing time and tracer clip simulations were run within CFD. Not only will this give visual validation of this ideology but it will also validate the theory that there is local build up of supersaturation at the feed point.

Tracer simulations were performed within Fluent and three separate tracer probes were created. These probes were positioned in various positions within the crystallizer (Probe 1 at FBRM window, Probe 2 at reactor base and Probe 3 was located at the liquid surface). The overall mixing time was calculated by averaging the three results. It is recommended within the literature that multiple probes are used so as to obtain a more realistic blend time¹⁴. For addition close to the impeller shaft ('near') a blend time of 1.1 seconds was obtained, this is in comparison to 1.4 seconds for addition close to the reactor wall ('far'). An increase in the anti-solvents blend time of ~30% has allowed for sufficient supersaturation to build up around the feed pipe, thus allowing for inconsistent MSZW and particle size results.

The combination of the blend times and the visual anti-solvent 'hold-up', produced from the tracer clips, allows for the variation in the MSZW data, with a change in feed location, to be fully understood. This increases process understanding at the laboratory scale and gives valuable information required for a successful and robust scale up.

Case Study 2: Location of 'Optimum' Feed Point Location through CFD

It is extremely important in anti-solvent crystallizations to minimise areas of high supersaturation around the region of the feed pipe (as shown in case study 1). Minimising supersaturation will prevent premature nucleation and increase both the crystallization robustness and repeatability. As mentioned in the literature, it is important to locate the addition of the anti-solvent in a region that is not only dominant in the downward velocity but also located in an area of prominent micromixing¹². Although CFD has difficulties in producing highly accurate turbulent kinetic energy values it is still useful for locating areas of turbulent mixing. The following profile is the local energy input at the liquid surface.

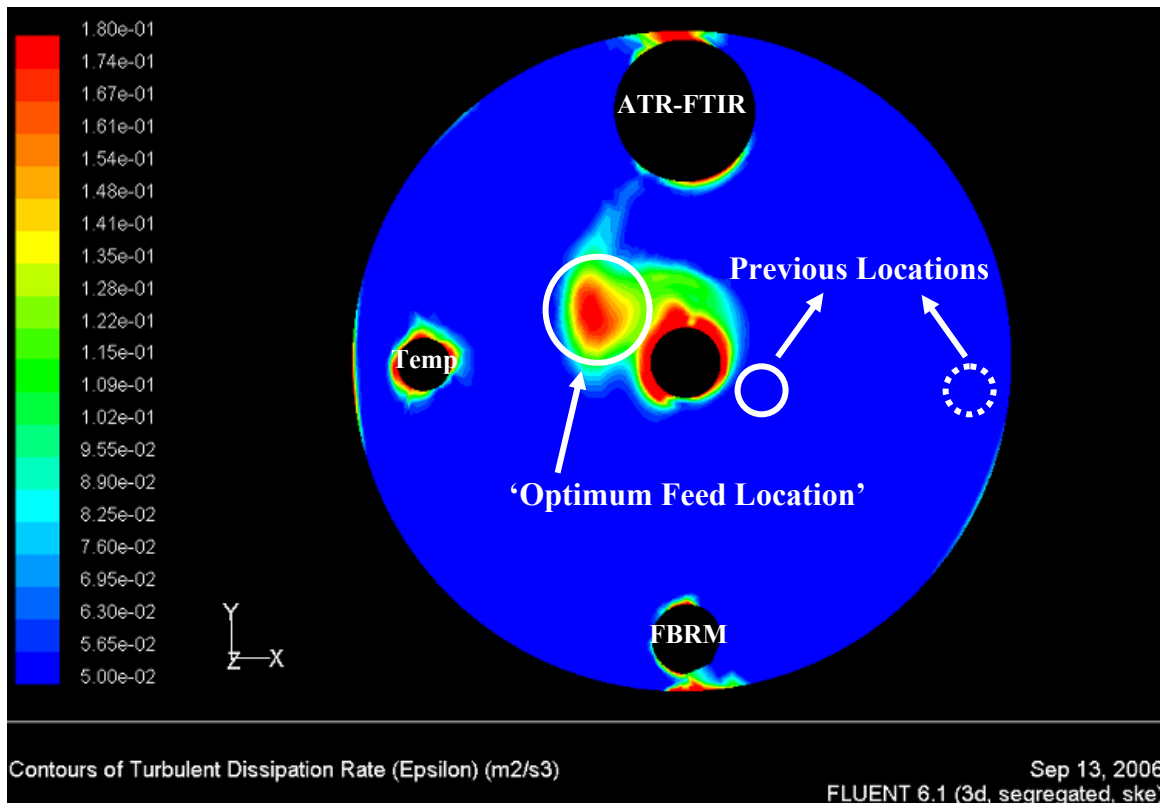


Figure 6: Local energy input for nucleation volume, at liquid surface at 325 rpm.

The highest local energy input can be found on the opposite side of the 500 ml reactor as the previous two addition points, and is in an area close to the impeller shaft and FTIR probe. This region has substantially higher local energy input and velocities in the negative-z direction (see figure 4, case study 1), hence the incorporation of the anti-solvent into the bulk solution and time taken to produce a homogenous mixture will be reduced still further (i.e. 'optimum feed point location').

By reducing the systems blend time and potentially increasing the systems homogeneity it is hoped to reduce MSZW fluctuations and increase both particle size and process robustness. Increasing ones particle size is a key objective within the pharmaceutical industry as it can reduce the impact on down stream processing, such as drying and filtration. Therefore, re-examining the crystallization at this point is warranted from an industrial troubleshooting perspective.

Various addition rates were examined to assess the impact on the MSZ and the CLDs. However, on addition in this region encrustation of the impeller shaft occurred. Encrustation is also common in cooling crystallizations, where there is a large temperature difference between the bulk solution and the reactor wall. This leads to high supersaturation at the wall, thus encrustation at the reactor wall can occur⁴. This same phenomenon was evident in this anti-solvent bench scale study.

In the present study the 'optimum' feed point is in a region of intense micromixing and addition of anti-solvent at this point caused splashing of saturated solution and anti-solvent onto the impeller shaft. This induced the crystallization of the benzoic acid onto the impeller shaft. This phenomenon was particularly evident at high addition rates ($0.24 \text{ g s}^{-1} - 0.48 \text{ g s}^{-1}$) and at a reduced agitation rate of 250 rpm. At the higher agitation of 325 rpm these seed crystals could not maintain contact with the impeller shaft and therefore encrustation was not always a problem. At 250 rpm the seed crystal deposition on the impeller shaft would continue to increase in size with anti-solvent addition. As the liquid volume within the reactor increased this seed deposition would eventually become immersed, at this point there are sufficient buoyant forces to force the deposition off the impeller shaft. This induced the sporadic and unpredictable seeding of the crystallization. In turn the process was less robust and results fluctuated.

The following image was taken prior to the seed deposit breaking off the impeller shaft.

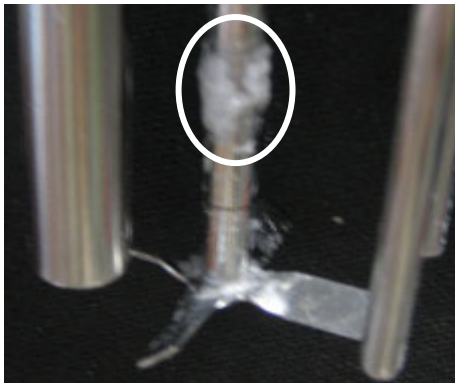


Figure 7: Impeller encrustation produced at 'optimum feed point location'.

The impact of the impeller encrustation was investigated using FBRM, as shown below.

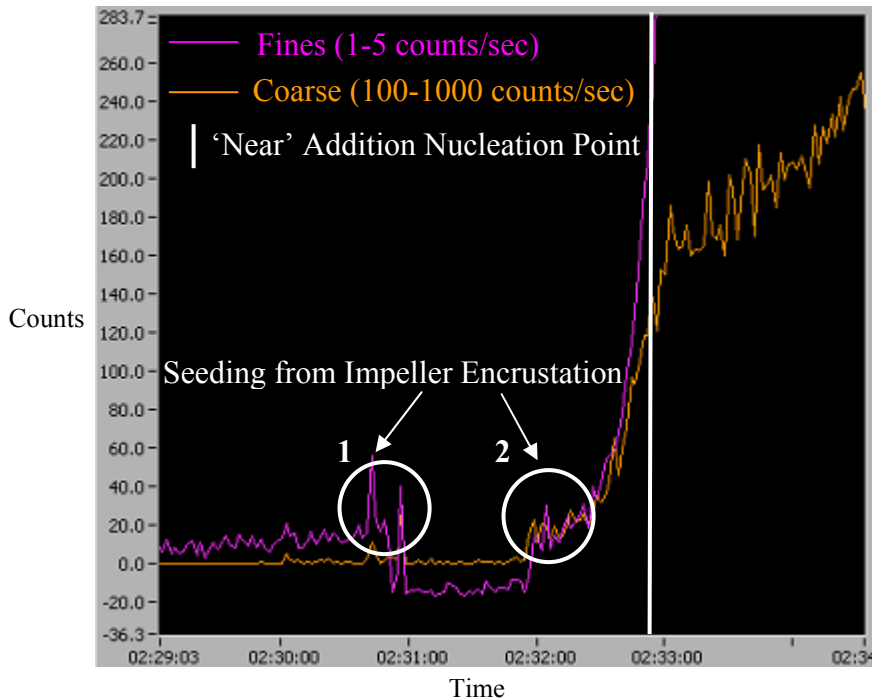


Figure 8: FBRM trend showing intermittent seeding of crystallizer

Figure 8 shows two cases of sporadic seeding from the impeller shaft at 250 rpm and an addition rate of 0.24 g s^{-1} . In case 1 the dispersed seed is re-dissolved in the bulk solution as there is sufficient solubility available. However, at point 2 the system is fully saturated and re-dissolution is not possible as the crystallization is operating close to the solubility curve. Seeding at this stage of the crystallization is extremely detrimental as it will induce premature nucleation and hence mimic the effects that were observed at the 'far' addition point in case study 1. Also shown in figure 8 is the average nucleation point, under the same process conditions, for the 'near' addition point. It can be concluded that addition in a region of intense micromixing has led to both the seeding and premature nucleation of the system, a reduction in particle size was also observed. On scale up the power input to crystallizers tends to decrease (unless a constant P/V is required), therefore it is highly likely that such encrustation would be observed, as sufficient agitation would not be available to prevent the seed deposits from growing.

Here the importance of this semi-quantitative approach for scale up and process understanding is highlighted. The application CFD here highlighted an area for improvement (anti-solvent addition location); however without bench scale tests, with *in-situ* tools, the true impact of changing ones addition point could not have been assessed. From a CFD modelling perspective this addition point should increase processes robustness, due to a reduction in blend time and thus a reduction in supersaturation gradients present in the crystallizer. However, after experimental analysis with FBRM it can be concluded that both modelling and experimental work our necessary prior to the relocation of ones feed point, be it at 500ml laboratory scale or at 70L pilot scale production.

Case Study 3: Nozzle Addition; Increasing Process Robustness & Reducing Impact of Poor Mixing

Nozzle addition is frequently applied in industrial scale crystallizers to help reduce the impact of poor mixing evident at large scales. As the relocation to the 'optimum feed point' failed the criterion for success (reduce MSZ fluctuations and increase particle size) it was decided to implement nozzle addition to the 'far' addition point in an effort to overcome the poor anti-solvent dispersion. In this study the normal feed pipe diameter was reduced from 5 mm to less than 1 mm. This in turn leads to an increase in the injection velocity of the anti-solvent to the crystallizer.

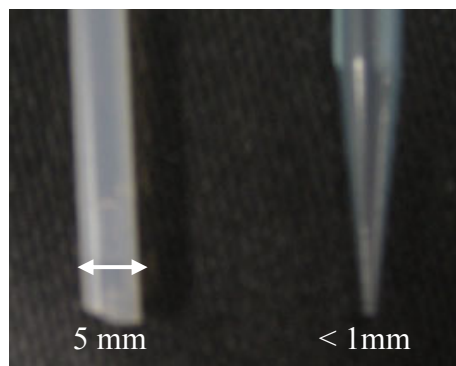


Figure 9: Normal/Nozzle Feed Pipes

| Addition (g/s) | 'Normal' Velocity (m/s) | 'Nozzle' Velocity (m/s) |
|----------------|-------------------------|-------------------------|
| 0.4779 | 0.01 | 0.15 |
| 0.334 | 0.0043 | 0.11 |
| 0.24 | 0.0031 | 0.08 |
| 0.144 | 0.0018 | 0.05 |
| 0.045 | 0.0006 | 0.01 |

Table 1: Exit velocities from 'Normal'/'Nozzle' Addition

With a reduction in the feed pipe diameter there is an increase in the anti-solvents exit velocity, as shown in table 1, and a reduction in the droplet diameter upon entry to the bulk solution. Both of these factors are crucial in reducing the regions of high supersaturation found in the region of the feed pipe (case study 1) and in decreasing the anti-solvents blend time. By increasing the exit velocity, the depth at which the anti-solvent penetrates the liquid surface increases, this is particularly evident from tracer experiments with high addition rates (0.33 and 0.48 g s⁻¹). This should aid in overcoming the poor local turbulent energy dissipation evident at the reactor wall (see figure 6, case study 2) and prevent the 'liquid hold-up', which was present with the normal addition mode. Additionally by reducing the droplet diameter of anti-solvent there is a reduction in the volume of anti-solvent that has to be dispersed in a specific time period. This in turn will allow for the production of a more homogeneous mixture (reducing high supersaturation gradients) and therefore allow for an increase in anti-solvent addition prior to nucleation (i.e. eliminate premature nucleation).

Nozzle MSZW Results

Due to the substantial fluctuations in the MSZW data present in case study 1, it was decided to re-characterize the crystallization at both 325 and 250 rpm at the 'far' feed point location.

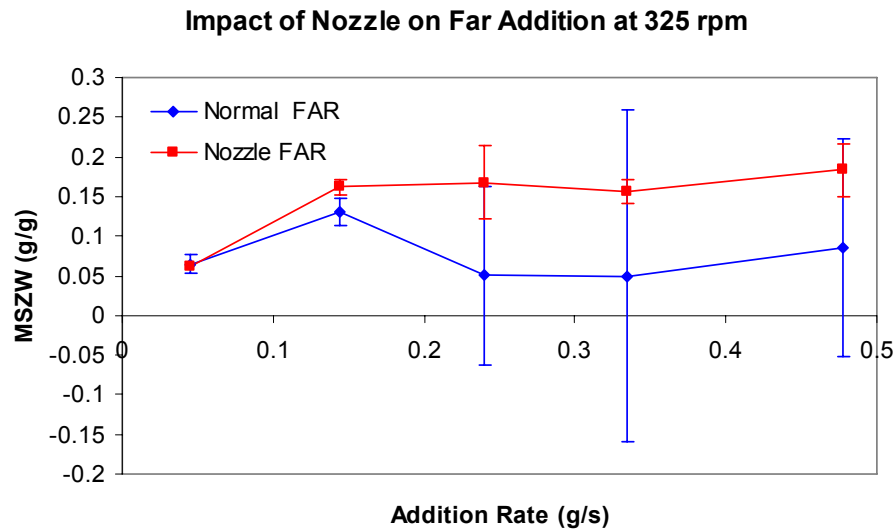


Figure 10: Impact of Nozzle Addition on MSZW at 'Far' Addition at 325 rpm

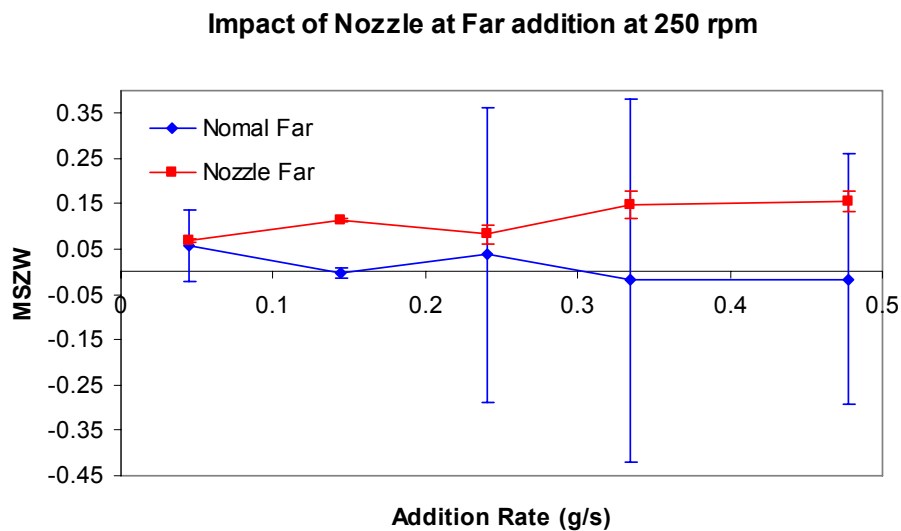


Figure 11: Impact of Nozzle Addition on MSZW at 'Far' Addition at 250 rpm

As shown by figures 10 and 11 the fluctuations observed at the 'far' addition location have been eliminated. In both cases the application of the nozzle to the addition of anti-solvent has prevented the premature nucleation of the system (i.e. negative MSZWs) as was observed in case study 1. The use of the nozzle has allowed for an increase in the MSZWs at both 325 and 250 rpm. The increased penetration depth, of the anti-solvent, and the reduction in droplet

size have allowed for increased dispersion and so a reduction in local supersaturation at the feed point. The supersaturation in both cases was not sufficient to induce premature nucleation as the system is more homogeneous. At some addition rates no error is produced over the course of three experiments, thus highlighting the positive impact that nozzle addition has had on the repeatability of the crystallizations at this small laboratory scale.

In the above cases the reduction in the feed pipes cross sectional area has allowed for the same trend, which was observed for 'near' addition (case study 1, figure 2 and 3), to be observed. An increase in MSZW is now evident with an increase in addition rate, even with the poor turbulent kinetic energy dissipation apparent at the reactor wall. Therefore, it can be concluded that the impact of poor mixing, in regions of anti-solvent additions, can be reduced/eliminated through the application of nozzle addition.

It is also apparent from the CFD profiles produced that the velocity patterns change as the liquid volume within the crystallizer increases. This was particularly evident at the 70L scale with a rushton turbine. As the velocity profiles shift so does the region for optimum anti-solvent addition (i.e. optimum feed point shifts from reactor wall to impeller shaft). Altering ones feed point during an industrial crystallization can be difficult, therefore nozzle addition can play an important role in overcoming poor mixing if the optimum feed location shifts during the crystallization. Therefore, a reduction in feed pipe diameter should be implemented in an effort to produce "right first time" scale up.

FBRM Trends and CLDs for Nozzle Addition

The MSZW data produced shows that there is an increase in the anti-solvent required for nucleation, as the mixture is more homogenous. Importantly the change in the systems supersaturation, from nozzle addition, needs to be quantified from a particle size perspective.

It is apparent from the MSZW data produced that the largest reduction in the MSZW fluctuations observed is at 325 rpm and 0.34 g s^{-1} . Therefore, the largest impact on the CLDs should be observed under these experimental criteria. The following trends/distributions were produced after a fixed addition time of 6 minutes and 1 sec and a hold time of 10 minutes after anti-solvent addition.

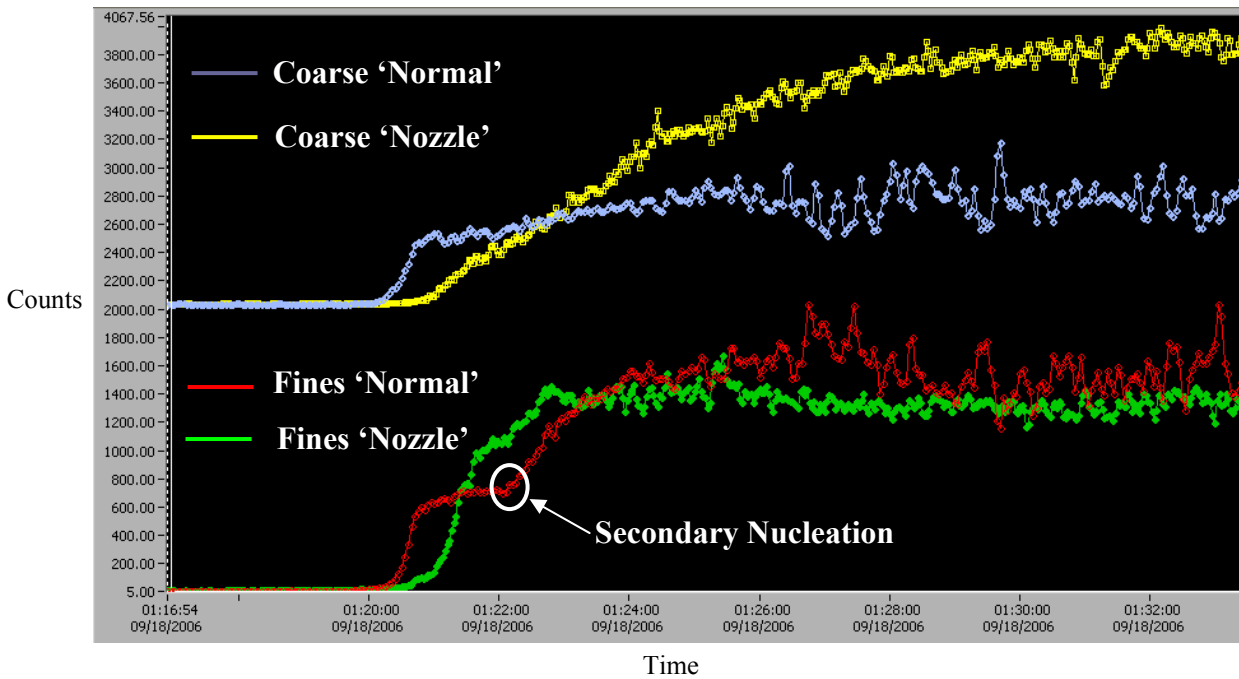


Figure 12: FBRM trends highlighting difference in nucleation and growth events for nozzle and normal addition

As shown above the nucleation event occurs at a later stage in the crystallization for nozzle addition. Also highlighted by the above figure is the elimination of the secondary nucleation event which is present with normal addition. By eliminating this event there is in turn a reduction in the fines produced. There is also a much slower growth dominated stage evident with nozzle addition; this in turn has led to a substantial increase in the coarse counts produced. As the supersaturation at the feed point has been reduced and a more homogenous system been created the kinetics are thermodynamically favored by growth, this explains for the increase in coarse counts and for the reduction in fines. This theory is further validated by analyzing both the CLDs produced from the FBRM probe and the microscope images taken for the same crystallization.

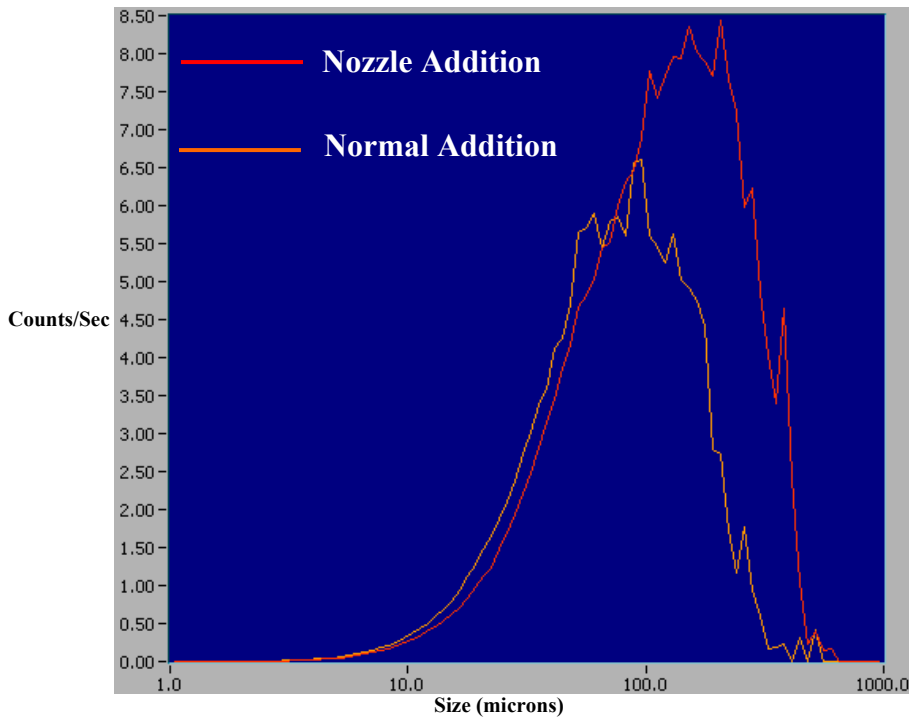


Figure 13: Square-weighted distribution for Nozzle and Normal feed pipe addition at 0.34 g s^{-1} at 325 rpm

As shown from figure 13 there is a distinct shift to the right for nozzle addition, thus indicating an increase in the systems particle size. The statistical information gathered from the FBRM probe also highlights this increase in coarse particles, and the decrease in fines produced due to the elimination of the secondary nucleation event (see table 2).

| | Normal | Nozzle | % Diff. |
|---|---------|---------|---------|
| Mean Square Weight ($1\mu\text{m} - 1000\mu\text{m}$) | 93.4 | 146.36 | 57 |
| Median No Weight ($1\mu\text{m} - 1000\mu\text{m}$) | 14.2 | 15.26 | 7 |
| #/sec ($1\mu\text{m} - 10\mu\text{m}$) | 3399.67 | 2633.66 | - 23 |
| #/sec ($100\mu\text{m} - 1000 \mu\text{m}$) | 192.56 | 334.17 | 74 |

Table 2: Statistical information showing difference in chord length distributions for normal and nozzle feed pipe diameters, for 'far' addition at 0.34 g s^{-1} at 325 rpm.

As shown above there is increase in coarse particles, which is highlighted by the mean square weight, by 57 % and a reduction in fines, which is highlighted by median no weight, by 7%. The count/sec data also emphasizes the change in the particle size with a decrease in fines ($1-10\mu\text{m}$) by 23% and an increase in coarse particle counts per second by 74%. Microscope images of the two crystallizations confirm the increase in particle size, with an obvious increase in the particles aspect ratio.

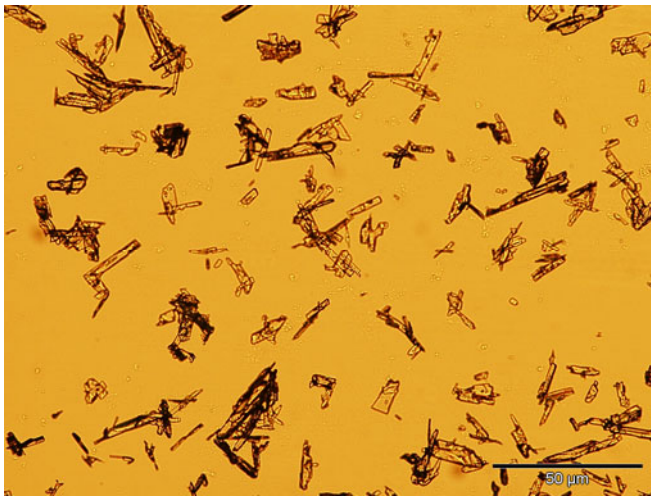


Figure 14: Normal Feed Addition

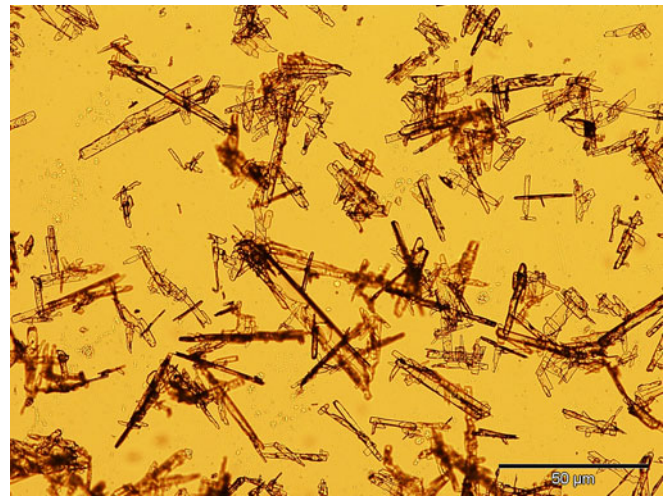


Figure 15: Nozzle Feed Addition

Thereby, it can be concluded that the systems supersaturation has been directly impacted and has allowed for the following changes in the systems crystallization characteristics.

- Increase in MSZWs at all addition rates.
- Elimination of premature nucleation
- Elimination of high fluctuations in MSZWs
- Reduced supersaturation at feed point
- Elimination of secondary nucleation
- Increase Particle size (57 % increase in coarse particles and 7% reduction in fines)
- Therefore, crystallizations robustness has increased and impact on down stream processing, such as drying and filtration, has been reduced.

Such positive results at the 'far' feed point location prompted the investigation of nozzle addition at the 'near' (well mixed) feed location. To assess the impact of the nozzle, in this well mixed region, it was decided to investigate the impact on particle size where there is little variation between the MSZW produced by the nozzle and normal addition. The slowest addition rate of 0.045 g s^{-1} and an agitation intensity of 325 rpm produce similar MSZWs. However, with such a small change in the MSZWs produced there is still a dramatic change in the particle size, even at these slow addition rates.

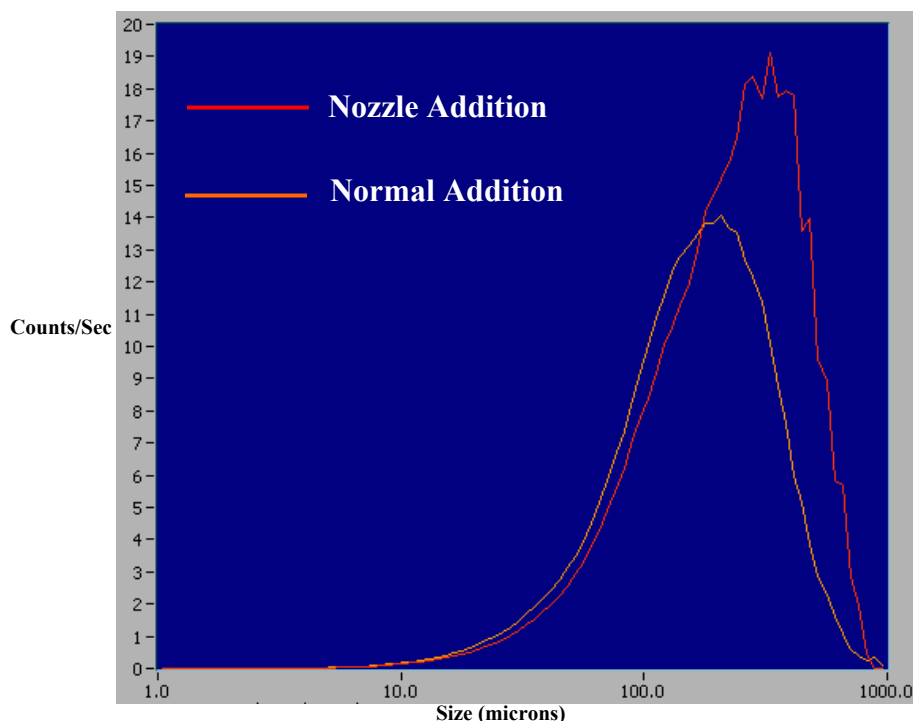


Figure 15: Square-weighted distribution for Nozzle and Normal feed pipe addition, at 0.045 g s^{-1} and 325 rpm at 'near' feed location

Again, even at lower addition rates this same increase in the systems particle size is evident with a shift in the CLDs to the right. Outlined below is the statistical information gathered from this crystallization.

| | Normal | Nozzle | % Diff. |
|---|---------|---------|---------|
| Mean Square Weight ($1\mu\text{m} - 1000\mu\text{m}$) | 195.89 | 261.78 | 34 |
| Median No Weight ($1\mu\text{m} - 1000\mu\text{m}$) | 19.92 | 20.34 | 2 |
| #/sec ($1\mu\text{m} - 10\mu\text{m}$) | 1524.13 | 1314.09 | -14 |
| #/sec ($100\mu\text{m} - 1000 \mu\text{m}$) | 537.13 | 550.88 | 3 |

Table 3: Statistical information showing difference in chord length distributions for normal and nozzle feed pipe diameters for 'near' addition at 0.045 g s^{-1} at 325 rpm.

A substantial increase of 34% is observed for the coarse particle, with a negligible decrease of 3% in fines. The change in the particle size is not as drastic as the previous example, due to the good dispersion of anti-solvent by 'normal' addition means at the low addition rate. But importantly it is still possible to improve ones crystallization, even with addition of anti-solvent in a well mixed region, through nozzle addition. This highlights the impact that local supersaturation at the feed point can play in determining the particle size of ones system. Therefore, an optimum addition mode and addition location needs to be considered prior to any scale up attempts.

Conclusions

The effect of anti-solvent addition rate, location and mode as well as agitation intensity on the anti-solvent crystallization of benzoic acid has been investigated. As shown a semi quantitative approach through the combination of *in-situ* tools and CFD is essential to gain process understanding for scale up. CFD allows for the mixing regime present within the crystallizer to be fully understood through velocity profiles, tracer simulations and mixing time results. This valuable information gained allows for minimal bench scale experiments to optimize a crystallization process.

Experimental data combined with CFD modelling indicates that addition close to the wall hinders the incorporation of anti-solvent resulting in areas of high supersaturation and premature nucleation. CFD quantitatively allowed for the location of the 'optimum feed point' for anti-solvent addition. However, due to the intense turbulent kinetic energy dissipation in this region splashing of solution onto the impeller shaft occurred, which in turn allowed for the encrustation of the shaft (see image 1). This reduced process control through sporadic seeding of the crystallization. This again highlighted the importance of the semi quantitative approach for examining crystallizations prior to scale up, as if experimental methods were abandoned at this stage a poor crystallization strategy would be achieved and eliminate any chance of "right first time" scale up.

Initial tracer experiments conducted at the 500mL and 70 L scale show that while incorporation of the anti-solvent at the small scale occurs very quickly at the large scale it takes some time and results in an area of high tracer concentration (supersaturation) close to the addition point. As shown in case study 3 nozzle addition overcame poor mixing at the 'far' addition location and increased the crystallizations repeatability and particle size. Therefore, at the pilot scale nozzle addition at multiple addition locations will help in overcoming the poor mixing present in the pilot scale crystallizer.

As shown at the bench scale mixing plays a crucial role in reducing supersaturation at the feed pipe. On scale up the importance of mixing will be further emphasized, therefore the following strategy will be applied,

- Application of CFD for location of 'optimal' feed point for anti-solvent at 2L and 70L scales (minimise blend time). Ensure no impeller/wall/baffle encrustation.
- Agitate at a maximum rate, which would not induce crystal breakage (determine at bench scale with CFD and *in-situ* tools).
- Increase number of feed points to overcome single regions of high supersaturation and premature nucleation
- Use Nozzle Addition at all feed points above surface to help minimise supersaturation gradients and to aid in overcoming poor mixing present at pilot scale. Also, incorporate subsurface addition to addition technique in the plane of the impeller.

References

1. Kougoulos *et al.* Modeling particle disruption of an organic fine chemical compound using Lasentec focussed beam reflectance monitoring (FBRM) in agitated suspensions. *Powder Technology*. 2005;155;153-158
- Kougoulos *et al.* CFD modeling of mixing and heat transfer in batch cooling crystallizations *Chem. Engineering Research and Design* 2005;83 (A1):30-39.
- Kougoulos *et al.* Process modeling tools for the continuous and batch organic crystallization processes including application to scale up 2006;10:739-750
2. Sha *et al.* Application of CFD simulation to suspension crystallization – factors affecting size-dependant classification. *Powder Technology*. 2001;121;20-25
3. Woo *et al.* Simulation of mixing effects in anti solvent crystallizations using a coupled CFD-PDF-PBE Approach *Crystal Growth and Design*. 2006;6;1291-1303
4. Schmidt *et al.* Application of Process Modeling Tools in the scale up of pharmaceutical crystallization processes *Organic Process Research and Development*. 2004;8:998-1008
5. Paul *et al.* Organic Crystallization Processes. *Powder Technology*. 2005;150:133-143
6. Barrett & Glennon. Characterizing the metastable zone width and solubility curve using Lasentec FBRM and PVM . *Chem. Engineering Research and Design*. 2002;80:799-805.
7. Shi *et al.* Effects of calcium and other ionic impurities on the primary nucleation of burkeite. *Industrial and Engineering Chemistry Research*. 2003;42:2861-2869
8. Doki *et al.* Process control of seeded batch cooling crystallization of the metastable alpha-form glycine using an in-situ ATR-FTIR spectrometer and an in-situ FBRM particle counter. *Crystal Growth and Design*. 2004;4;949-953
9. Scott & Black. In-line analysis of impurity effects an crystallization. *Organic Process Research and Development*. 2005;9:890-893
10. Liotta & Sabesan. Monitoring and feedback control of supersaturation using ATR-FTIR to produce an active pharmaceutical ingredient of a desired crystal size. *Organic Process Research and Development*. 2004;8:488-494
11. Lewiner *et al.* Improving batch cooling seeded crystallization of an organic weed-killer using on-line ATR FTIR measurement of supersaturation. *Journal of Crystal Growth*. 2001b;226;348-362
12. Groen & Roberts. Nucleation, growth, and pseudo-polymorphic behavior of citric acid as monitored in situ by attenuated total reflection Fourier transform infrared spectroscopy. *Journal of Physical Chemistry B*. 2001;105;10723-10730

13. *Perry, R. H.* Perry Chemical Engineerings' Handbook 6th Edition 1984

14. *Bujalski et al.* The influence of the addition position of a tracer on CFD simulation mixing times in a vessel agitated by a rushton turbine. Trans IChemE;80 (A):824-831